ACS Energy Letters

Caltech Library

Subscriber access provided by Caltech Library

Letter

Effects of Surface Roughness on the Electrochemical Reduction of CO2 over Cu

Kun Jiang, Yufeng Huang, Guosong Zeng, Francesca M. Toma, William A. Goddard, and Alexis T. Bell

ACS Energy Lett., **Just Accepted Manuscript** • DOI: 10.1021/acsenergylett.0c00482 • Publication Date (Web): 19 Mar 2020

Effects of Surface Roughness on the Electrochemical Reduction of CO_2 over Cu

Kun Jiang,[1,2,3†] Yufeng Huang,[4†] Guosong Zeng,[5] Francesca M. Toma,[2,5]
William A. Goddard, III,[4] and Alexis T. Bell*[2,3,5]

[1]Institute of Fuel Cells, School of Mechanical Engineering, Shanghai Jiao Tong University, Shanghai, 200240

[2]Joint Center for Artificial Photosynthesis, Lawrence Berkeley National Laboratory, Berkeley, California 94720

[3]Department of Chemical and Biomolecular Engineering, University of California, Berkeley, California 94720

[4]Materials Simulation Center and Joint Center for Artificial Photosynthesis, California Institute of Technology, Pasadena, California 91125

[5]Chemical Sciences Division, Lawrence Berkeley National Laboratory, Berkeley, California 94720

[†]These authors contributed equally to this work.

Submitted to
ACS Energy Letters

*To whom correspondence should be sent: alexbell@berkeley.edu

Abstract

We have investigated the role of surface roughening on the CO_2 reduction reaction (CO_2RR) over Cu. The activity and product selectivity of Cu surfaces roughened by plasma pretreatment in Ar, O_2, or N_2 were compared with that of electrochemically polished Cu those. Differences in total and product current densities, the ratio of current densities for HER (the hydrogen evolution reaction) to CO_2RR, and the ratio of current densities for C_{2+} to C_1 products depend on the electrochemically active surface and are nearly independent of plasma composition. Theoretical analysis of an electropolished and roughened Cu surface reveals a higher fraction of undercoordinated Cu sites on the roughened surface, sites that bind CO preferentially. Roughened surfaces also contain square sites similar to those on a Cu(100) surface but with neighboring step sites, which adsorb OC-COH, a precursor to C_{2+} products. These findings explain the increases in the formation of oxygenates and hydrocarbons relative to CO and the ratio of oxygenates to hydrocarbons observed with increasing surface roughness.

Electrochemical CO_2 reduction reaction (CO_2RR) offers a promising route for the production of chemicals and fuels using renewable electricity generated from wind and solar energy.[1-4] Among metallic electrocatalysts evaluated for this purpose, copper is the only metal that produces hydrocarbons and oxygenated products with high Faradaic efficiency (FE).[5-10] Previous studies have shown that the activity and selectivity of Cu are strongly dependent on the surface morphology of the metal, as well as its local reaction environment (electrolyte composition and pH).[11-16] For example, Cu(100) and Cu(211) surfaces are more active than Cu(111) surfaces and more effective in promoting C-C bond formation on both single crystal Cu electrodes[17, 18] and Cu nanoparticles.[19, 20] Recent theoretical calculations have shown that square sites of Cu(100) bind *OCCO and *OCCHO more strongly than do sites on Cu(111), and that the step sites of Cu(211) facilitate the kinetics of CO dimerization relative to those on Cu(111), resulting in a higher C_{2+}/C_1 selectivity on square and stepped facets.[21, 22] The role of other low-coordination Cu sites beyond those present on low-index facets is the subject of continuing discussion. An investigation of the CO_2RR over size-controlled Cu nanoparticles has also shown that the population of low-coordination Cu surface sites increases with decreasing Cu particle size (from 15 nm to 2 nm), and that high coordination site result in higher H_2 and CO selectivities and lower hydrocarbon (CH_4 and C_2H_4) selectivities.[23] By contrast, a comparative investigation of CO_2RR on (100)-, (111)-, and (751)-preferentially orientated Cu thin film electrodes revealed that both Cu(100) and (751) surfaces with Cu coordination numbers from 6 to 8 promote C-C bond formation relative to more highly coordinated sites on Cu(111) surfaces.[24] More recently, a study of the electrochemical reduction of CO has suggested that highly porous Cu electrode could favor C_{2+} oxygenates selectivity with a large suppression of competitive HER; however, the underlying causes for these observations remains unclear.[25]

Oxide-derived Cu with enriched surface grain boundaries have also been reported to be efficient for reducing CO_2 to multi-carbon products.[26-29] It has been hypothesized that this enhanced C_{2+} products selectivity on oxide-derived Cu could arise from surface Cu^+ retained under reaction conditions and stabilized by subsurface oxygen[28, 30] or adsorbed halide anions,[31, 32] e.g., I^-, based on *quasi in situ* spectroscopic experiments. However, this hypothesis has been challenged by recent DFT calculations,[33, 34] ^{18}O labeling,[35] electrochemical Raman spectroscopy[36, 37] and *in situ* synchrotron XAS and XRD experiments,[38, 39] suggesting the near-surface oxygen and/or Cu(I) species are not sufficiently long-lived to be present under reaction conditions at highly reducing

cathode potentials.[40] A more plausible interpretation for the enhanced C_{2+} selectivity of oxide-derived Cu is offered by a recent theoretical analysis of sites present on a rough Cu nanoparticle. This work concludes that surface twin boundaries in the oxide-derived Cu associated with concave defects with respect to Cu(100) planes serve as active sites for C-C bond formation by stabilizing OC-COH species, one of the precursors to C_{2+} products.[41]

In this study, we investigate the effects of plasma pretreatment of polished Cu foils in different gas atmospheres on their CO_2RR activity and selectivity. Since O_2-plasma treatment will cause both chemical and physical modifications to Cu surfaces, we pretreated Cu by Ar^+ ion bombardment in an Ar plasma in order to isolate the effects of surface roughening. These studies show that the changes in the distribution of CO_2RR products is attributable to changes Cu surface topography created by the plasma pre-treatments. Roughened Cu surfaces containing a high proportion of under-coordinated Cu sites that exhibit stronger CO adsorption energies than more highly coordinated site present of planar surfaces. Consistent with this finding, the fraction of CO formed from CO_2 released as CO decreases and the fraction converted to hydrocarbons and alcohols increases with increasing roughness. Our experimental efforts are supported by an analysis of the distribution of sites on a simulated roughened surface of Cu. This work shows that the roughened surface contains a much higher proportion of under-coordinated sites, and in particular sites that adsorb OCCOH, a suggested precursor to C_{2+} products,[41] more strongly than do the more highly coordinated sites present on a Cu(100) surface.

Surface Characterization Before and After Plasma Pre-treatment

Figures 1A and 1B show atomic force microscopy (AFM) and scanning electron microscopy (SEM) images, respectively of the electrochemically polished Cu foil. Fig. 1C presents the AFM topography image of Cu foil after 10-min Ar plasma treatment. In contrast to the polished foil, the Ar plasma-treated foil is much rougher, exhibiting extensive ridges and valleys.[42] The arithmetic surface roughness factor (S_a) increases from 1.28 nm for the electropolished foil to 7.68 nm after Ar^+ sputtering based on an AFM scan of a 500 nm x 500 nm area (Fig. S1). SEM images of Ar plasma treated Cu foil before and after CO_2RR electrolysis are shown in Fig. 1D. In agreement with the topography determined by AFM, the 2D projection exhibits a surface structure

covered with pits and islands generated by Ar^+ bombarding and re-deposition of Cu atoms. Similar surface roughening effects were also observed for N_2 and O_2 plasma treated Cu foils (Fig. S2).

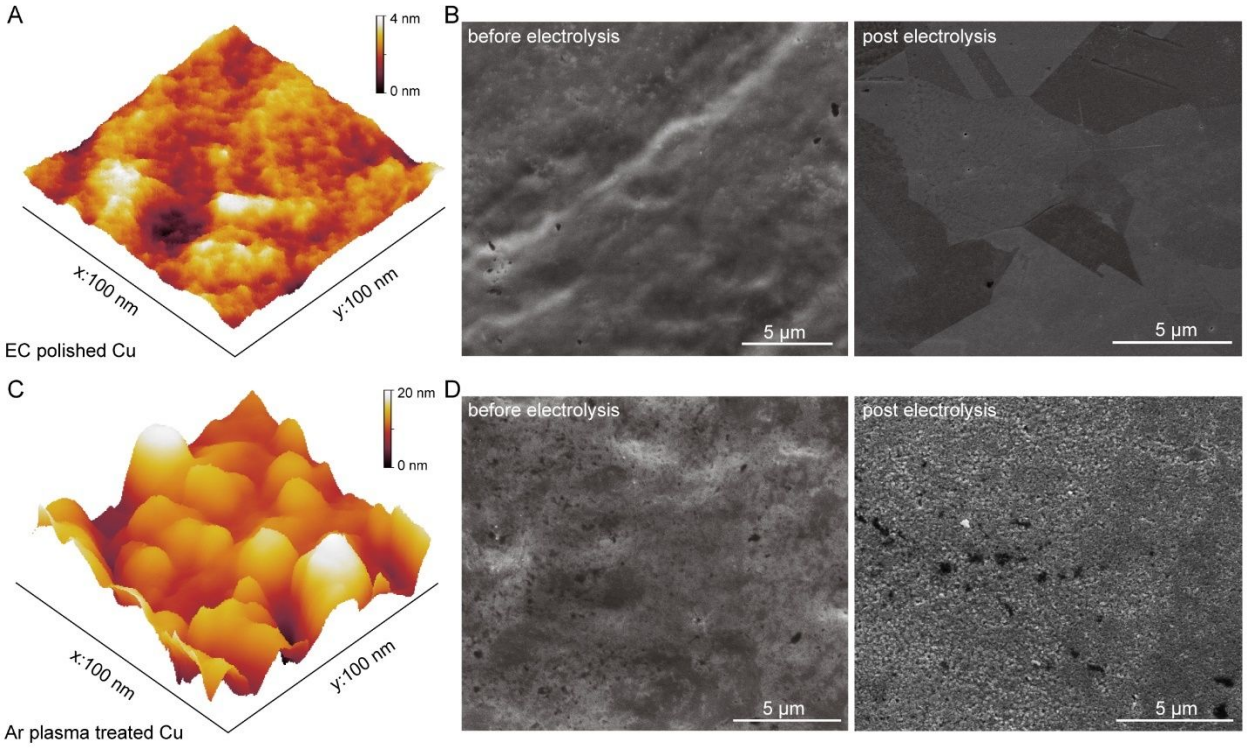

Figure 1. Cu electrodes characterization. AFM and SEM images of electrochemically polished Cu foil (A, B) acquired before and after a 10-min plasma pre-treatment in Ar. Images (A) and (C) show the reconstructed 3D topography of the surface obtained from AFM scans, images (B) and (D) show typical SEM images of Cu foils taken before and after 1-h CO_2RR electrolysis at -1.0 V in CO_2-saturated 0.1 M $CsHCO_3$.

To further quantify the surface roughness of Cu foils electrodes, we determined the electrochemically active surface area (ECSA) by measuring the double-layer capacitances and then calculating the relative roughness of plasma pre-treated Cu compared to electropolished Cu (Table 1 and Fig. S3). In general, all of the plasma treatments increased the roughness of Cu, and prolonged pretreatment time led to a more roughened surface. For the same pretreatment duration, Cu foils treated in either an Ar or O_2 plasma were rougher than that exposed to an N_2 plasma. These differences are likely due to the larger ion size of Ar^+, the more aggressive etching of O^{2-},[43, 44] as well as the pronounced surface structural rearrangement caused by removal of oxygen from copper oxide during electrochemical reduction.[26, 34] We also note that plasma pretreatment in an

N_2 plasma for more than 10 min did not increase the surface roughness of Cu further, in contrast to what was observed for pretreatment in an O_2 plasma.

Table 1. Determined surface roughness of post electrolysis Cu foils with different plasma pretreatments.

Electrode	Electro-polished	N_2 Plasma	Ar Plasma			O_2 Plasma		
		10-min	5-min	10-min	20-min	5-min	10-min	20-min
Roughness	1.00	1.57	1.42	2.58	3.64	1.85	2.92	3.93

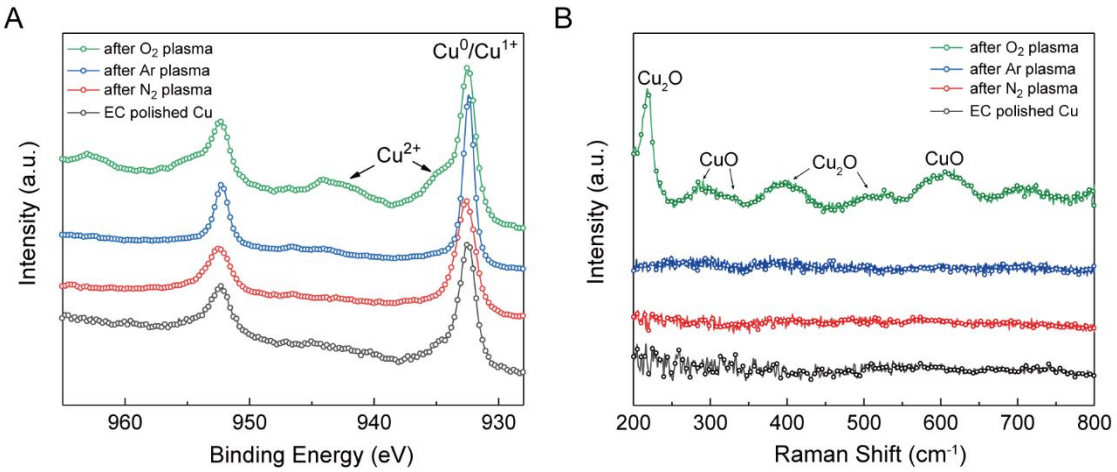

Figure 2. Chemical state characterization of Cu electrodes. *Ex situ* (A) XPS and (B) Raman spectra recorded on Cu foils after 10-min plasma treatments under different gaseous atmosphere.

Figure 2A shows the *ex-situ* core level X-ray photoelectron spectra (XPS) of the Cu 2p region after plasma treatments in different atmospheres. All four samples show the predominant peak at 932.4 (Cu $2p_{3/2}$) and 952.2 eV (Cu $2p_{1/2}$), corresponding to Cu(0) or Cu(I). For the O_2 plasma treated Cu, two other satellite peaks show up at ~935 eV and ~944 eV, which are assigned to Cu(II) species. Evidence for Cu(II) cation was also obtained from the Cu LMM region of the Auger spectrum (see Fig. S4). Raman spectra of these four Cu samples are shown in Fig. 2B. No obvious Raman scattering feature is observed for electropolished Cu or Cu exposed to a N_2 or an Ar plasma. By contrast, features for both Cu_2O (~218, 402 and 526 cm^{-1}) and CuO (~290, 332 and 617 cm^{-1}) are observed after O_2 plasma pretreatment,[45] in agreement with XPS spectra and Raman studies reported previously.[28, 32]

Electrochemical Activity and Selectivity

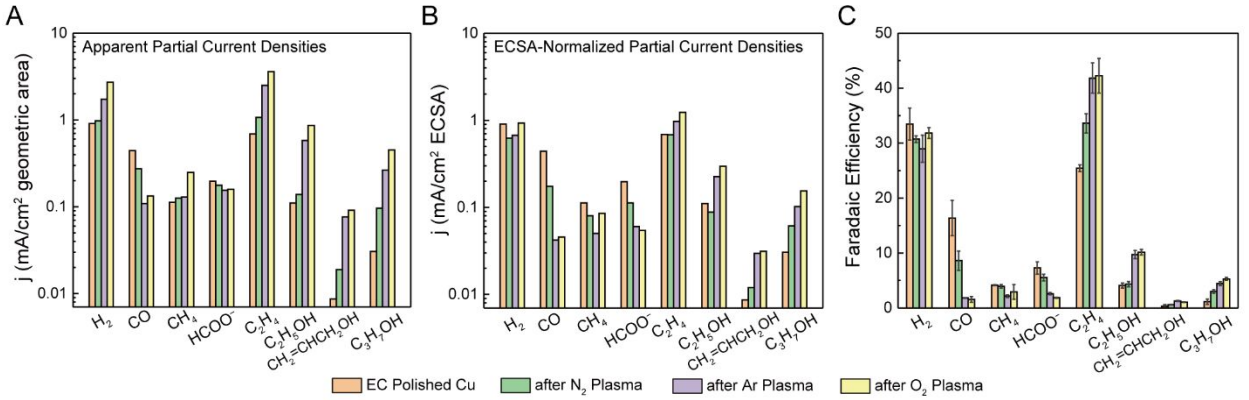

Figure 3. Electrochemical reduction of CO_2 over Cu foil electrodes after 10-min plasma pretreatments under different gaseous atmosphere. (A) Geometric area normalized, (B) ECSA-normalized partial current densities and (C) selectivity of major products during CO_2RR over Cu foil electrodes after 10-min plasma pre-treatments under different atmosphere.

The electrochemical CO_2RR performance of plasma pre-treated Cu foils was evaluated by 1-h chronoamperometric electrolysis at -1.0 V vs. RHE, for which the CO_2 consumption rate is below 17.0 nmol s^{-1} cm^{-2} (Fig. S5).[46] 0.1 M $CsHCO_3$ was employed as the supporting electrolyte, based upon our previous studies showing that Cs^+ cations enhance the field stabilization of the intermediates critical to the formation C_2 products[13, 14, 47] (further evidence for influence of cation identity is given in Fig. S6). The superficial current densities shown in Fig. 3A all increase with plasma pretreatment, in the order of the increasing ECSA. To account for this effect, Fig. 3B shows the current densities for all four samples normalized by the ECSA. The ECSA-normalized current densities for H_2 and CH_4 are not strongly changed by plasma pretreatment, whereas those for CO and $HCOO^-$ decreases and those for all C_{2+} product increases in the order no pretreatment < N_2 plasma pretreatment < Ar plasma pretreatment < O_2 plasma pretreatment. We note in particular that the rate of CO evolution decreases by more than an order of magnitude upon Ar or O_2 plasma pretreated Cu compared to that for electropolished Cu, and the rate of C_3 products generation - allyl alcohol and n-propanol - increases by a factor of 3 to 5. The FEs of the principal products of the CO_2RR generated on electropolished and plasma pretreated Cu are illustrated in Fig. 3C. After 10-min plasma pretreatment, the selectivity toward hydrogen evolution (HER) and methane generation does not change very much, while the FEs for CO and $HCOO^-$ decrease in the order of

polished Cu > N_2 plasma pretreated Cu > Ar plasma pretreated Cu ≈ O_2 plasma pretreated Cu. By contrast, the FEs for C_{2+} products - C_2H_4, C_2H_5OH and n-propanol - follow the reverse trend.

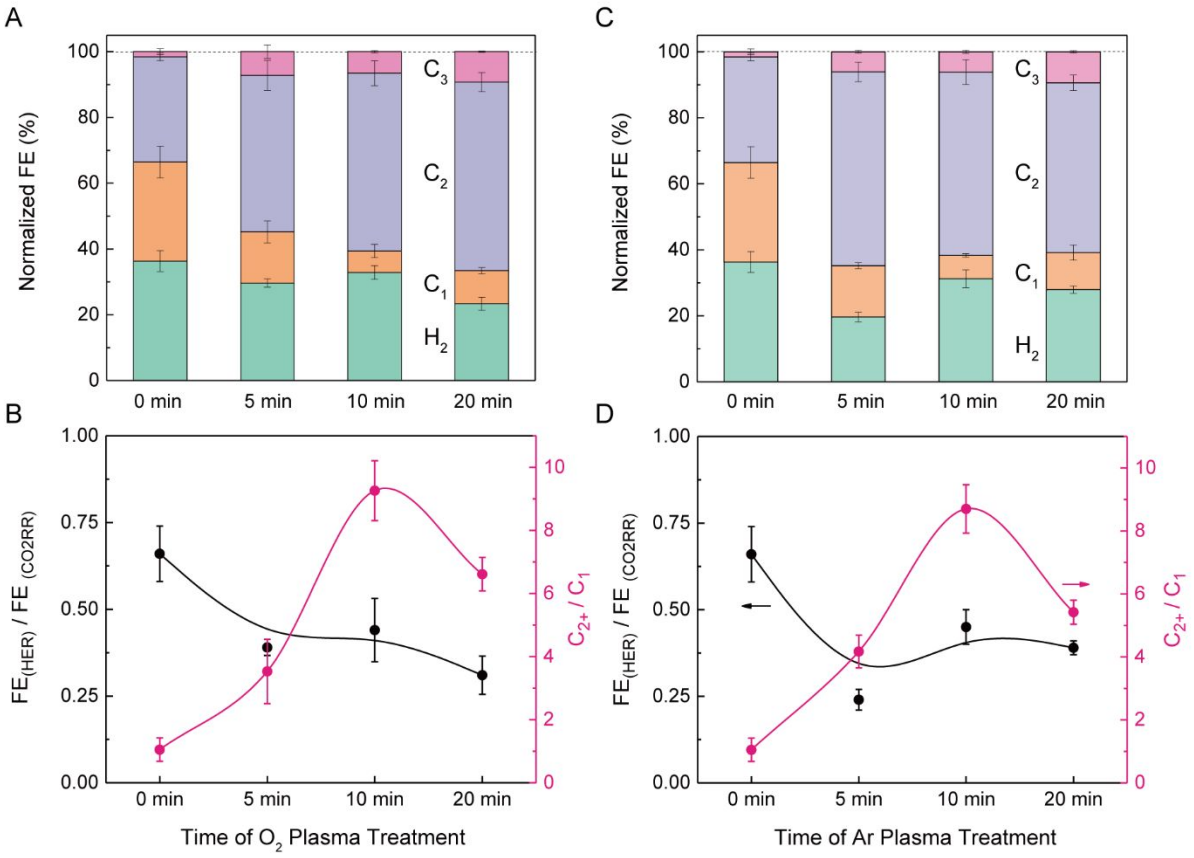

Figure 4. CO_2RR products distribution as a function of plasma treatment time. Both (A, B) O_2 and (C, D) Ar atmosphere plasma pretreatments were plotted. The sum of as-determined overall FEs are varied from 92.2% to 98.9% and all normalized to 100% in panels (A) and (C) for comparison.

The similarity of both C_{2+} product selectivities and specific activities of Cu after Ar or O_2 pretreatment is particularly interesting. Therefore, we investigated the effects of the duration of plasma pretreatment in Ar and O_2 on the distribution of CO_2RR products. Fig. 4 shows these results for durations of 0, 5 10, and 20 min, with the electropolished sample referenced as 0-min. The normalized FEs (referenced to 100%) are given in Figs. 4A and 4C. The FE for HER is cyan column, the FE for C_1 products ($HCOO^-$, CO and CH_4) is orange column, the FE for C_2 products (C_2H_4 and C_2H_5OH) is purple column, and the FE for C_3 products (allyl alcohol and n-propanol) is magenta column. The selectivity ratio of HER/CO_2RR (black line) and the C_{2+}/C_1 ratio (red line) are illustrated in Figs. 4B and 4D. We observe similar product distributions throughout the time-

course for both O_2 and Ar plasma pre-treatments, which could largely rule out the (sub)surface oxygen effect. HER decreases to below 30% after 5-min plasma exposure in both cases and levels off with prolonged exposure. The FE for C_1 products also decreases from 0 to 10 min, then increases again due to enhanced methane evolution after a 20-min pretreatment. Over the same pretreatment time, the FE for C_3 alcohols reaches ~10%, whereas the FE for C_{2+} products rises to ~60%. The ratio of C_{2+}/C_1 reaches a maximum value of ~9 after 10-min of pretreatment in either an Ar or O_2 plasma.

Since the Cu surface roughness increases with prolonged plasma-treatment time, we assessed whether the changes shown in Fig. 4 correlate with surface roughness. The choice of which product ratios to plot is guided by recent theoretical studies of the CO_2RR mechanism, which suggest that $2e^-$ products ($HCOO^-$ and CO_g) are produced via the adsorbed intermediates *HCOO and *COOH, respectively, whereas both CH_4 and C_{2+} products are produced via the reduction of *CO.[5, 6, 48-51] Therefore, as illustrated in Fig. 5A, *CO serves as the key intermediate to CH_4 and C_{2+} products. Figures 5B and 5C plot the selectivity ratios for C_{2+} products versus C_1 products ($HCOO^-$, CO, and CH_4) and versus CH_4 alone, respectively. The C_{2+}/C_1 ratio reaches a value of ~9 for a roughness of ~3 and then decreases thereafter, regardless of whether Cu is pretreated in an Ar or O_2 plasma. By contrast, the C_{2+}/CH_4 ratio increases monotonically to a value of 30 in the case of Ar plasma pretreatment but reaches a maximum value of ~20 and then decreases in the case of O_2 pretreatment.

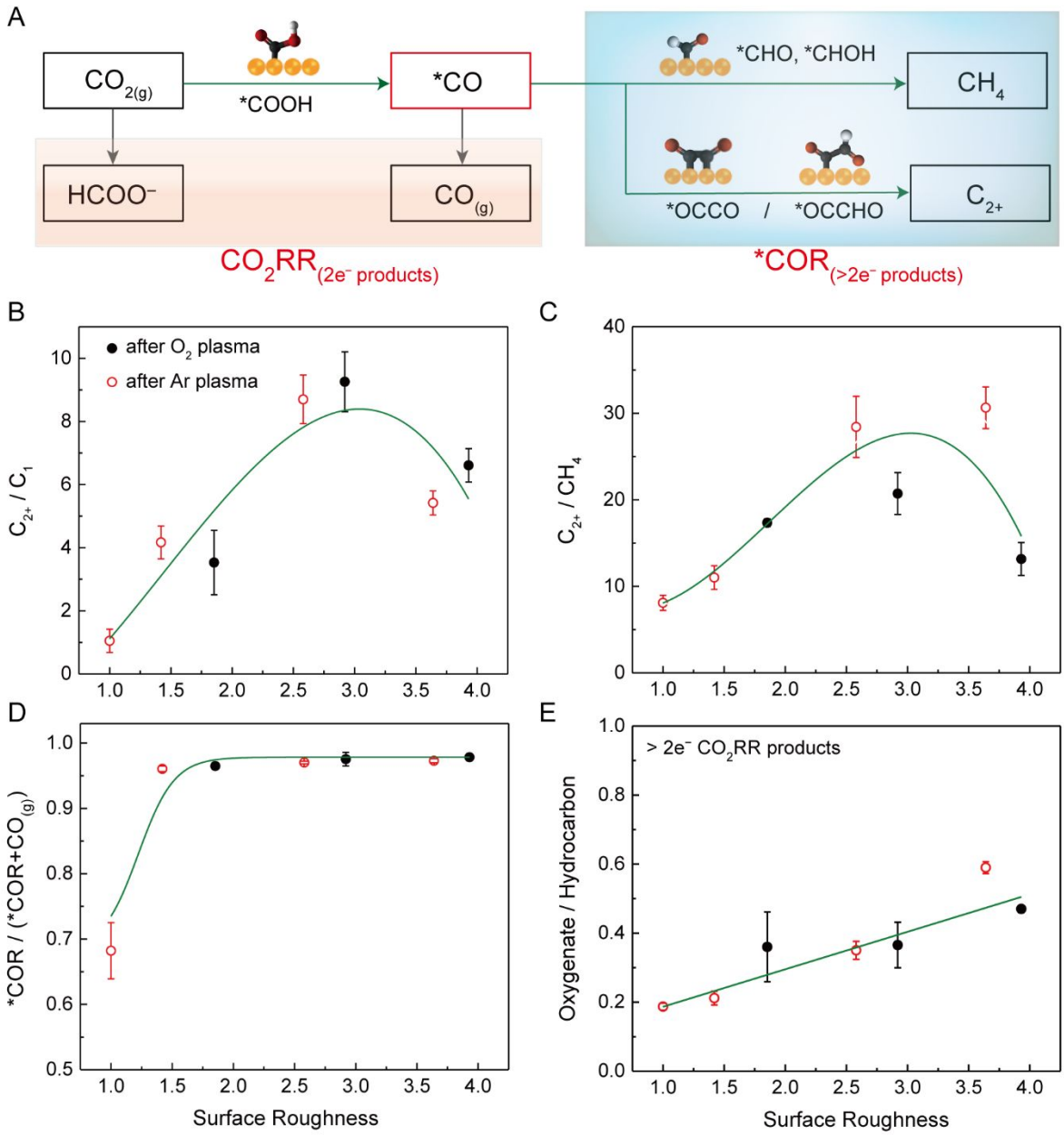

Figure 5. CO_2RR products distribution as a function of Cu surface roughness. (A) Simplified flowchart of CO_2RR mechanism leading to C_1 and C_{2+} products generation, * corresponds to adsorbed species, >2e reduction products of CH_4 and C_{2+} that go through the reduction of *CO intermediate (*COR) are marked in light blue. (B) C_{2+}/C_1 ratio, (C) C_{2+}/C_{CH4} ratio, (D) $*COR/(CO_{(g)} + *COR)$ ratio, and (E) oxygenate/hydrocarbon (only >2e reduction products) ratio.

Figure 5D show that the fraction of CO produced by the CO_2RR converted to CH_4 and C_{2+} products increases from 0.68 for a roughness of 1.0 to 0.96 for a roughness of 1.5. Further increasing the roughness to ~4.0 increases this ratio to 0.98. The trend observed in Fig. 5D suggests

that the binding energy for CO increases monotonically with surface roughness, consistent with temperature-programmed desorption experiments[26] and recent theoretical calculations on simulated Cu particle surface.[41, 52] The theoretical work also predicts that the stability of *OC-COH, a critical precursor to C_2 products, increases with surface roughness and in particular with the formation of concave sites at grain boundaries between Cu(100) and Cu(111) surfaces. The downturn in the ratio of FEs for C_{2+} product formation and CH_4 formation seen in Fig. 5C when the roughness exceeds ~3.0 for O_2 plasma pretreated Cu might be attributable to the formation of sub-nanometric Cu clusters (i.e., surface dimer and trimer adatoms) that could serve as active sites for selective CO_2-to-CH_4 conversion.[53] Finally, Fig. 5E shows the surface roughness dependence of the ratio of FEs for C_{2+} oxygenated products to that for C_{2+} hydrocarbons. The selectivity to C_{2+} oxygenated products (ethanol, allyl alcohol and n-propanol) increases by a factor of two with increasing roughness, most likely due to the lower surface coverage by *H, as reflected in the HER trend of Fig. 4, and the reduced likelihood of hydrogenating C–C intermediates on the roughened Cu surfaces. Similarly, the selectivity to $HCOO^-$ decreases as the roughness increases from 1.0 to 2.6, and levels off thereafter (Fig. S7). We suggest that this trend is due to the lower availability of terrace sites on roughened Cu surfaces, which are needed to bond bidentate *HCOO, the precursor to HCOOH and hence $HCOO^-$ upon desorption of HCOOH into the alkaline electrolyte.[6]

A further factor that can contribute to enhancing the ratio of C_{2+}/CH_4 on roughened vs smooth Cu surfaces is the higher local pH near the surface of the roughened Cu; therefore, we considered the possible effect of pH on the observed results. The higher pH near the roughened surface is ascribable to the higher rate of OH^- generation rate per geometric electrode area. We note that this proposal is consistent with the control experiment presented in Fig. S8, illustrating the effects of increased bicarbonate concentration, and the earlier findings of Hori et al., who reported a 4-fold enhancement in the C_{2+}/CH_4 ratio upon increasing the surface pH from 8.5 to 9.5.[54] In our studies, we observed only a ~2.6-fold increase in the C_{2+}/CH_4 ratio due to an estimated increase in the surface pH change from 9.76 to 9.88 for Cu treated for 5-min vs. 10-min in an Ar plasma. The pH for these experiments was estimated assuming a mass-transfer boundary layer thickness of ~40 μm and a bicarbonate concentration of 0.1 M.[46, 55] We also note that it has been reported that the increase in surface pH as a consequence of electrolyte polarization should suppress CH_4 production, but keep C_{2+} activity constant at a given potential.[56, 57] Figure 3B shows that while the intrinsic activity (ECSA-normalized partial current density) for forming CH_4 decreases following plasma

pretreatment, the intrinsic activities for producing C_{2+} products, especially oxygenated products, increases. These observations suggest that the enhanced C_{2+} selectivity observed after plasma treatment is not attributable to the small change in the local pH.

Table S1 compares our results on the effects of surface roughness with those previously reported. Various methods have been used to roughen the surface of Cu. These include reduction of copper oxides produced by thermal and/or plasma oxidation, potential cycling in halogen-containing solutions, dendrite growth, etc. Regardless of the method used to achieve roughening, increased surface roughness generally leads to an enhanced C_{2+} FE and C_{2+}/C_1 ratio. Most authors have attributed these effects enhanced surface roughness to a greater abundance of under-coordinated surface sites and defective sites that bind *CO strongly and promote its further reduction to C-C bond formation. Unfortunately, these results cannot be compared with those reported here because of large difference in the modes of sample preparation and conditions for their inveistgation.

Theoretical Simulation and Analysis

Insights into why surface roughening causes an increase in the formation of C_{2+} products can be gained by atomic-level analysis of the Cu surface created by computational simulation of Ar^+ bombardment roughening of a Cu(111) surface followed by thermal relaxation of the resulting surface. The simulation of roughening begins with a 17.6 nm × 17.4 nm surface that 10.1 nm thick, which contains ~ 5,422 total surface atoms (see Fig. 6A). Figure 6B and the Supporting Movie 1 show that after bombardment of this surface with 1300 Ar^+ cations, the Cu surface exposes 10,433 atoms, corresponding to an increase in surface roughness of 1.93. The simulated untreated Cu surface and the plasma-treated surface resemble the topography and roughness of the experimental observations, as seen in Figure 1.

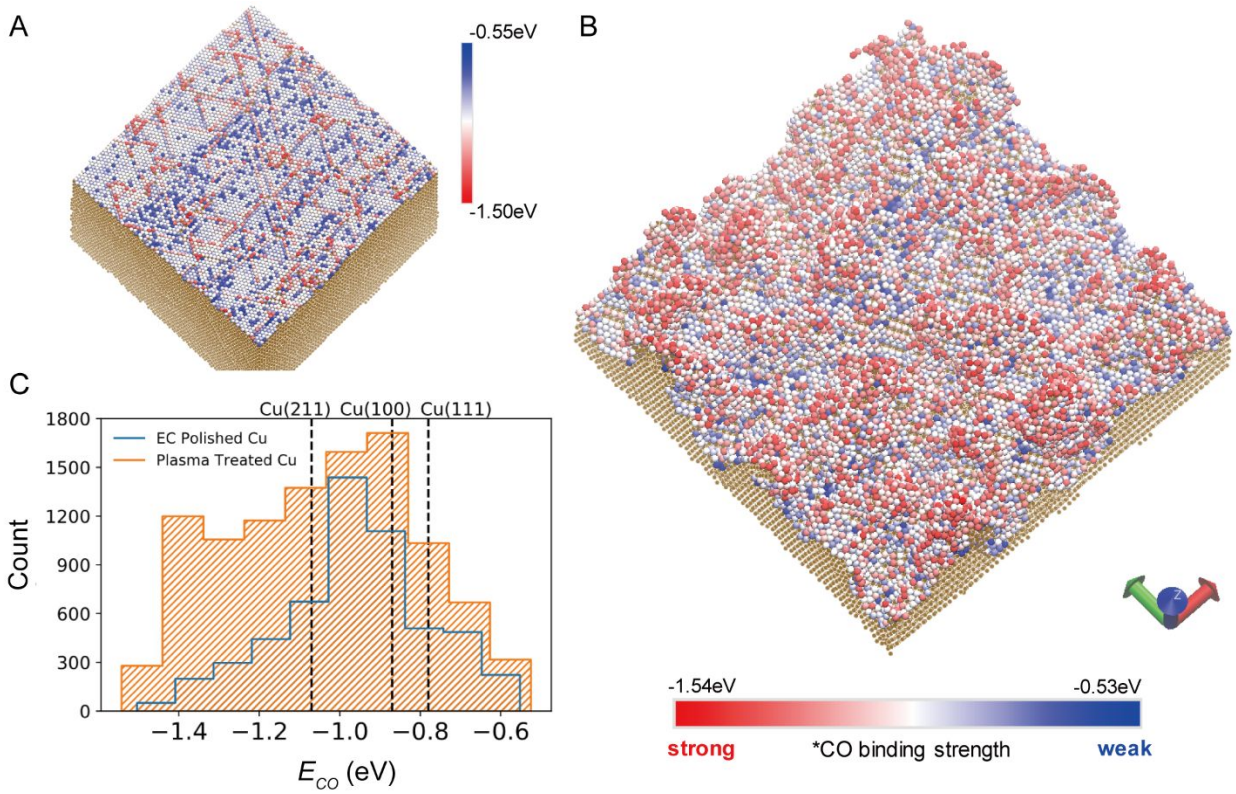

Figure 6. Active site visualization by ReaxQM-Machine Learning. Images of the computationally produced Cu surface of (A) electro-polished and (B) after Ar plasma bombardment, and (C) predicted distribution of CO adsorption energies, ΔE_{CO}. The three dashed lines indicate the CO adsorption energies on Cu(111), (100) and (211).

The ReaxQM-Machine Learning approach was used to predict the distribution of CO binding energies, ΔE_{CO}, for both simulated electrochemically polished Cu and the Ar plasma roughened surfaces.[41, 58] The electropolished Cu, shown in Fig. 6A, is dominated by close-packed low index sites, and, therefore, the mean values of ΔE_{CO} are close to those of Cu(111), (100) and (211) surfaces (Fig. 6C). By contrast, a much higher population of stronger CO binding sites, ranging from -1.10 to -1.54 eV (red sites along the ridges in Fig. 6B and the columns left of the Cu(211) line in Fig. 6C), appear after plasma pretreatment. The increased number of strong CO binding sites is consistent with the experimental observation of a reduced selectivity to CO formation following plasma pretreatment to roughen the catalyst surface. Since the adsorption of *CO and *H are expected to compete on the surface of Cu, the stronger adsorption of CO on roughened Cu is expected to result in a reduction of the *H/*CO. This reasoning would explain the increase in

the formation of oxygenated relative to hydrocarbon products observed with increasing roughening seen in Fig. 5E.

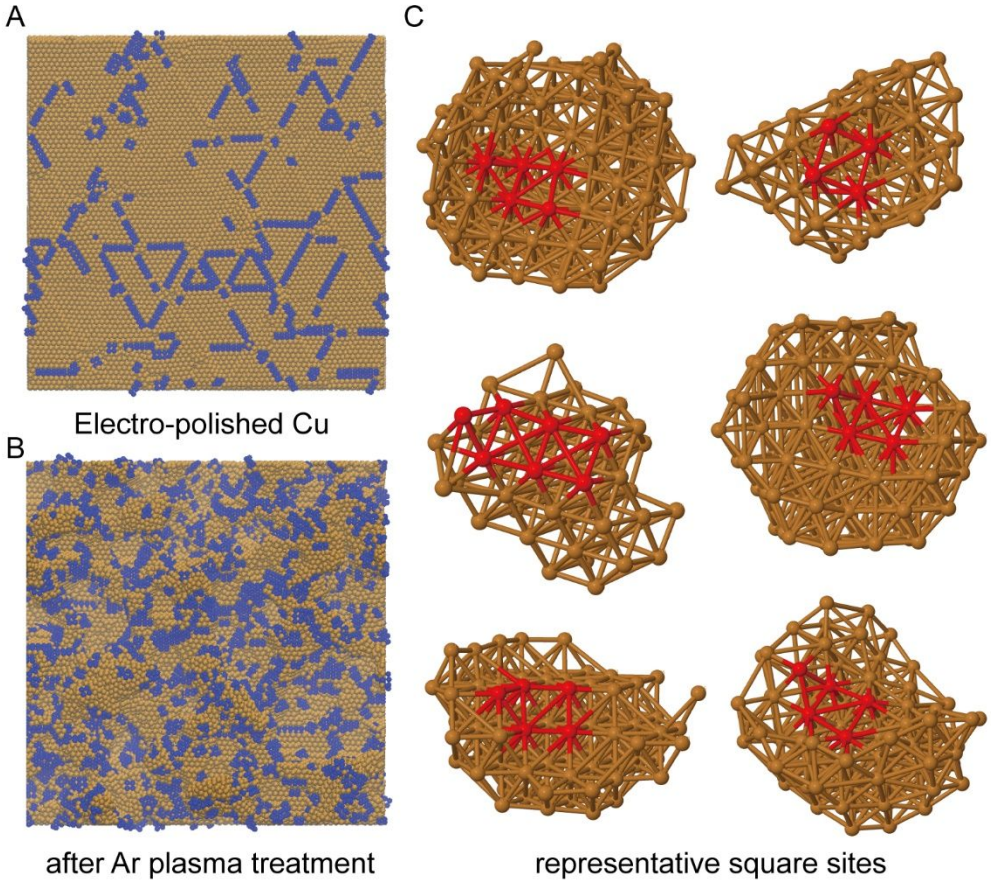

Figure 7. Visualization of square sites on computationally simulated Cu surfaces. (A) Electropolished Cu and (B) Ar plasma pretreated Cu, the surface square sites are marked in blue color. (C) Zoomed-in atomic structure of randomly chosen square sites on the plasma-treated Cu surface, both the square sites and the neighboring Cu step sites (if any) are highlighted in red.

In our previous work we have employed the formation energy of *OC-COH (ΔE_{OCCOH}) as a descriptor for the selectivity of C_{2+} products formed during the CO_2RR, and have shown that the mean value of ΔE_{OCCOH} decreased from ~1.35 eV for random surface sites to ~0.50 eV for surface square sites.[39] We also noted that concave defects located at Cu(100) plane next to a (111) step exhibited the most favorable values of ΔE_{OCCOH} for C_{2+} selectivity. In the present study, we identified the surface square sites on the simulated Cu surfaces for comparison as shown in Fig. 7A and 7B. The percentage of square sites to overall surface atoms increased from 20.9% on the

polished Cu surface to 38.5% on the surface produced by Ar plasma pretreatment. Fig. 7C shows the atomic structures of randomly chosen square sites occurring on the simulated surface produced by plasma treatment. The sites are similar to the Cu(100) configuration but have abundant neighboring step sites. As noted, the significantly increased percentage of surface square sites favors C-C bond formation and provides a rational for the enhanced C_{2+} selectivity that correlates with increased surface roughening caused by plasma pretreatment.

In conclusion, the present study investigated the effects of surface topography on the activity and product selectivity of electrochemical CO_2 reaction, demonstrating the distribution of products produced by CO_2RR on metallic Cu changes with Cu surface topography created by plasma pretreatment. The activity and product selectivity of electrochemically polished Cu was compared with those of roughened Cu surfaces prepared by different plasma pretreatments. The differences in overall CO_2RR activity from different plasma pretreatments are attributable changes in the electrochemically active surface area. Of particular note, we observe that with increasing surface roughness, the ratio of current densities for CO_2RR to HER, the ratio of the current densities for COR to the sum of the current densities for CO formation and COR, and the ratio of current densities for formation oxygenates to hydrocarbons all increase. These trends are interpreted based on an atomic-level analysis of the topogrphy of roughened Cu surface. We find that CO formed by the electrochemical reduction of CO_2 binds more strongly on the roughened surface than on the electrochemically polished surface, suggesting that the ratio of adsorbed H to CO decreases with increasing surface roughness. These trends explain why the fraction of CO produced by CO_2 reduction converted to reduced products and the fraction of these products appearing as oxygenates rather than hydrocarbons increase with increasing surface roughness. A further effect of increasing surface roughness is an increase in the fraction of final products (oxygenates and hydrocarbons) containing two or more C atoms. Our analysis shows that surface roughening increases the fraction of square sites similar to those on a Cu(100) surface but having abundant neighboring step sites. Prior work has shown that such sites enhance the formation of C-C bonds required to form C_{2+} products during the electrochemical reduction of CO_2. Finally, we find that increased roughening of the Cu surface increases the ratio of current densities for C_{2+} to C_1 (CO, $HCOO^-$, and CH_4) products up to a maximum value of ~ 9 for a surface roughness of ~ 3. Most of this downturn is ascribed to the enhanced formation of CH_4 on surfaces with roughness in excess of 3. The enhanced formation of methane on highly roughened surfaces is attributed to the formation of

surface dimer and trimer clusters on the Cu surface that have been shown by theoretical calculation to serve as active sites for selective conversion of CO_2 to CH_4. In summary, the results of the present work highlight the importance of surface topography and defect sites on the observed CO_2 reduction activity and selectivity, and suggest that rational surface structure engineering could contribute to the development of Cu electrocatalysts exhibiting a high selectivity to multi-carbon products.

Supporting Information

The Supporting Information is available free of charge on the ACS Publications website at DOI: xxx

Experimental and computational details; additional Cu electrodes characterization by AFM, SEM, Auger, XPS and electrochemical double-layer capacitance measurements; Cu surface roughness dependence of CO_2 consumption rate and $FE_{formate}/FE_{(COg+COR)}$ ratio during chronoamperometric electrolysis; online differential electrochemical mass spectrometry study on the cation effect; control experiments study on anion buffering effect and extra surface roughening at the presence of iodide anion

Acknowledgements

This material is based upon work performed by the Joint Center for Artificial Photosynthesis, a DOE Energy Innovation Hub, supported through the Office of Science of the U.S. Department of Energy under Award Number DE-SC0004993. We would also like to acknowledge Ms. Lien-Chun Weng, Dr. Zhou Lin and Prof. Martin Head-Gordon for insightful discussions.

References

1. De Luna, P.; Hahn, C.; Higgins, D.; Jaffer, S. A.; Jaramillo, T. F.; Sargent, E. H., What would it take for renewably powered electrosynthesis to displace petrochemical processes? *Science* **2019,** *364* (6438), eaav3506.
2. Shih, C. F.; Zhang, T.; Li, J.; Bai, C., Powering the Future with Liquid Sunshine. *Joule* **2018,** *2* (10), 1925-1949.
3. Jouny, M.; Luc, W.; Jiao, F., General Techno-Economic Analysis of CO_2 Electrolysis Systems. *Ind. Eng. Chem. Res.* **2018,** *57* (6), 2165-2177.

4. Verma, S.; Kim, B.; Jhong, H.; Ma, S. C.; Kenis, P. J. A., A Gross-Margin Model for Defining Technoeconomic Benchmarks in the Electroreduction of CO_2. *ChemSusChem* **2016,** *9* (15), 1972-1979.
5. Hori, Y.; Wakebe, H.; Tsukamoto, T.; Koga, O., Electrocatalytic Process of Co Selectivity in Electrochemical Reduction of CO_2 at Metal-Electrodes in Aqueous-Media. *Electrochim. Acta* **1994,** *39* (11-12), 1833-1839.
6. Kortlever, R.; Shen, J.; Schouten, K. J. P.; Calle-Vallejo, F.; Koper, M. T. M., Catalysts and Reaction Pathways for the Electrochemical Reduction of Carbon Dioxide. *J. Phys. Chem. Lett.* **2015,** *6* (20), 4073-4082.
7. Zhu, D. D.; Liu, J. L.; Qiao, S. Z., Recent Advances in Inorganic Heterogeneous Electrocatalysts for Reduction of Carbon Dioxide. *Adv. Mater.* **2016,** *28* (18), 3423-3452.
8. Xu, S.; Carter, E. A., Theoretical Insights into Heterogeneous (Photo)electrochemical CO_2 Reduction. *Chem. Rev.* **2019,** *119* (11), 6631-6669.
9. Gao, D.; Arán-Ais, R. M.; Jeon, H. S.; Roldan Cuenya, B., Rational catalyst and electrolyte design for CO_2 electroreduction towards multicarbon products. *Nat. Catal.* **2019,** *2* (3), 198-210.
10. Nitopi, S.; Bertheussen, E.; Scott, S. B.; Liu, X.; Engstfeld, A. K.; Horch, S.; Seger, B.; Stephens, I. E. L.; Chan, K.; Hahn, C.; Norskov, J. K.; Jaramillo, T. F.; Chorkendorff, I., Progress and Perspectives of Electrochemical CO_2 Reduction on Copper in Aqueous Electrolyte. *Chem. Rev.* **2019**, *119* (12), 7610-7672.
11. Pérez-Gallent, E.; Marcandalli, G.; Figueiredo, M. C.; Calle-Vallejo, F.; Koper, M. T. M., Structure- and Potential-Dependent Cation Effects on CO Reduction at Copper Single-Crystal Electrodes. *J. Am. Chem. Soc.* **2017,** *139* (45), 16412-16419.
12. Kim, D.; Kley, C. S.; Li, Y.; Yang, P., Copper nanoparticle ensembles for selective electroreduction of CO_2 to C_2–C_3 products. *Proc. Natl. Acad. Sci. USA* **2017,** *114* (40), 10560-10565.
13. Resasco, J.; Chen, L. D.; Clark, E.; Tsai, C.; Hahn, C.; Jaramillo, T. F.; Chan, K.; Bell, A. T., Promoter Effects of Alkali Metal Cations on the Electrochemical Reduction of Carbon Dioxide. *J. Am. Chem. Soc.* **2017,** *139* (32), 11277-11287.
14. Singh, M. R.; Kwon, Y.; Lum, Y.; Ager, J. W.; Bell, A. T., Hydrolysis of Electrolyte Cations Enhances the Electrochemical Reduction of CO_2 over Ag and Cu. *J. Am. Chem. Soc.* **2016,** *138* (39), 13006-13012.
15. Roberts, F. S.; Kuhl, K. P.; Nilsson, A., Electroreduction of Carbon Monoxide Over a Copper Nanocube Catalyst: Surface Structure and pH Dependence on Selectivity. *ChemCatChem* **2016,** *8* (6), 1119-1124.
16. Kas, R.; Kortlever, R.; Yilmaz, H.; Koper, M. T. M.; Mul, G., Manipulating the Hydrocarbon Selectivity of Copper Nanoparticles in CO_2 Electroreduction by Process Conditions. *ChemElectroChem* **2015,** *2* (3), 354-358.
17. Hori, Y.; Takahashi, I.; Koga, O.; Hoshi, N., Selective Formation of C_2 Compounds from Electrochemical Reduction of CO_2 at a Series of Copper Single Crystal Electrodes. *J. Phys. Chem. B* **2002,** *106* (1), 15-17.
18. Huang, Y.; Handoko, A. D.; Hirunsit, P.; Yeo, B. S., Electrochemical Reduction of CO_2 Using Copper Single-Crystal Surfaces: Effects of CO* Coverage on the Selective Formation of Ethylene. *ACS Catal.* **2017,** *7* (3), 1749-1756.
19. Loiudice, A.; Lobaccaro, P.; Kamali, E. A.; Thao, T.; Huang, B. H.; Ager, J. W.; Buonsanti, R., Tailoring Copper Nanocrystals towards C-2 Products in Electrochemical CO_2 Reduction. *Angew. Chem. Int. Edit.* **2016,** *55* (19), 5789-5792.
20. Jiang, K.; Sandberg, R. B.; Akey, A. J.; Liu, X.; Bell, D. C.; Nørskov, J. K.; Chan, K.; Wang, H., Metal Ion Cycling of Cu Foil for Selective C-C Coupling in Electrochemical CO_2 Reduction. *Nat. Catal.* **2018,** *1*, 111-119.
21. Schouten, K. J. P.; Pérez Gallent, E.; Koper, M. T. M., Structure Sensitivity of the Electrochemical Reduction of Carbon Monoxide on Copper Single Crystals. *ACS Catal.* **2013,** *3* (6), 1292-1295.
22. Sandberg, R. B.; Montoya, J. H.; Chan, K.; Nørskov, J. K., CO-CO coupling on Cu facets: Coverage, strain and field effects. *Surf. Sci.* **2016,** *654*, 56-62.
23. Reske, R.; Mistry, H.; Behafarid, F.; Roldan Cuenya, B.; Strasser, P., Particle Size Effects in the Catalytic Electroreduction of CO_2 on Cu Nanoparticles. *J. Am. Chem. Soc.* **2014,** *136* (19), 6978-6986.

24. Hahn, C.; Hatsukade, T.; Kim, Y. G.; Vailionis, A.; Baricuatro, J. H.; Higgins, D. C.; Nitopi, S. A.; Soriaga, M. P.; Jaramillo, T. F., Engineering Cu surfaces for the electrocatalytic conversion of CO_2: Controlling selectivity toward oxygenates and hydrocarbons. *Proc. Natl. Acad. Sci. USA* **2017,** *114* (23), 5918-5923.
25. Wang, L.; Nitopi, S.; Wong, A. B.; Snider, J. L.; Nielander, A. C.; Morales-Guio, C. G.; Orazov, M.; Higgins, D. C.; Hahn, C.; Jaramillo, T. F., Electrochemically converting carbon monoxide to liquid fuels by directing selectivity with electrode surface area. *Nat. Catal.* **2019,** *2* (8), 702-708.
26. Verdaguer-Casadevall, A.; Li, C. W.; Johansson, T. P.; Scott, S. B.; McKeown, J. T.; Kumar, M.; Stephens, I. E. L.; Kanan, M. W.; Chorkendorff, I., Probing the Active Surface Sites for CO Reduction on Oxide-Derived Copper Electrocatalysts. *J. Am. Chem. Soc.* **2015,** *137* (31), 9808-9811.
27. Ren, D.; Deng, Y. L.; Handoko, A. D.; Chen, C. S.; Malkhandi, S.; Yeo, B. S., Selective Electrochemical Reduction of Carbon Dioxide to Ethylene and Ethanol on Copper(I) Oxide Catalysts. *ACS Catal.* **2015,** *5* (5), 2814-2821.
28. Mistry, H.; Varela, A. S.; Bonifacio, C. S.; Zegkinoglou, I.; Sinev, I.; Choi, Y. W.; Kisslinger, K.; Stach, E. A.; Yang, J. C.; Strasser, P.; Cuenya, B. R., Highly selective plasma-activated copper catalysts for carbon dioxide reduction to ethylene. *Nat. Commun.* **2016,** *7*, 12123.
29. Lum, Y.; Yue, B.; Lobaccaro, P.; Bell, A. T.; Ager, J. W., Optimizing C–C Coupling on Oxide-Derived Copper Catalysts for Electrochemical CO_2 Reduction. *J. Phys. Chem. C* **2017,** *121* (26), 14191-14203.
30. Eilert, A.; Cavalca, F.; Roberts, F. S.; Osterwalder, J.; Liu, C.; Favaro, M.; Crumlin, E. J.; Ogasawara, H.; Friebel, D.; Pettersson, L. G. M.; Nilsson, A., Subsurface Oxygen in Oxide-Derived Copper Electrocatalysts for Carbon Dioxide Reduction. *J. Phys. Chem. Lett.* **2017,** *8* (1), 285-290.
31. Gao, D. F.; Zegkinoglou, I.; Divins, N. J.; Scholten, F.; Sinev, I.; Grosse, P.; Cuenya, B. R., Plasma-Activated Copper Nanocube Catalysts for Efficient Carbon Dioxide Electroreduction to Hydrocarbons and Alcohols. *ACS Nano* **2017,** *11* (5), 4825-4831.
32. Gao, D. F.; McCrum, I. T.; Deo, S.; Choi, Y. W.; Scholten, F.; Wan, W. M.; Chen, J. G. G.; Janik, M. J.; Cuenya, B. R., Activity and Selectivity Control in CO_2 Electroreduction to Multicarbon Products over CuO_x Catalysts via Electrolyte Design. *ACS Catal.* **2018,** *8* (11), 10012-10020.
33. Garza, A. J.; Bell, A. T.; Head-Gordon, M., Is Subsurface Oxygen Necessary for the Electrochemical Reduction of CO_2 on Copper? *J. Phys. Chem. Lett.* **2018,** *9* (3), 601-606.
34. Fields, M.; Hong, X.; Nørskov, J. K.; Chan, K., Role of Subsurface Oxygen on Cu Surfaces for CO2 Electrochemical Reduction. *J. Phys. Chem. C* **2018,** *122* (28), 16209-16215.
35. Lum, Y. W.; Ager, J. W., Stability of Residual Oxides in Oxide-Derived Copper Catalysts for Electrochemical CO_2 Reduction Investigated with O-18 Labeling. *Angew. Chem. Int. Edit.* **2018,** *57* (2), 551-554.
36. Kibria, M. G.; Dinh, C.-T.; Seifitokaldani, A.; De Luna, P.; Burdyny, T.; Quintero-Bermudez, R.; Ross, M. B.; Bushuyev, O. S.; García de Arquer, F. P.; Yang, P.; Sinton, D.; Sargent, E. H., A Surface Reconstruction Route to High Productivity and Selectivity in CO_2 Electroreduction toward C_{2+} Hydrocarbons. *Adv. Mater.* **2018,** *30* (49), 1804867.
37. Mandal, L.; Yang, K. R.; Motapothula, M. R.; Ren, D.; Lobaccaro, P.; Patra, A.; Sherburne, M.; Batista, V. S.; Yeo, B. S.; Ager, J. W.; Martin, J.; Venkatesan, T., Investigating the Role of Copper Oxide in Electrochemical CO_2 Reduction in Real Time. *ACS Appl. Mater. Interfaces* **2018,** *10* (10), 8574-8584.
38. Farmand, M.; Landers, A. T.; Lin, J. C.; Feaster, J. T.; Beeman, J. W.; Ye, Y.; Clark, E. L.; Higgins, D.; Yano, J.; Davis, R. C.; Mehta, A.; Jaramillo, T. F.; Hahn, C.; Drisdell, W. S., Electrochemical flow cell enabling operando probing of electrocatalyst surfaces by X-ray spectroscopy and diffraction. *Phys. Chem. Chem. Phys.* **2019,** *21* (10), 5402-5408.
39. Scott, S. B.; Hogg, T. V.; Landers, A. T.; Maagaard, T.; Bertheussen, E.; Lin, J. C.; Davis, R. C.; Beeman, J. W.; Higgins, D.; Drisdell, W. S.; Hahn, C.; Mehta, A.; Seger, B.; Jaramillo, T. F.; Chorkendorff, I., Absence of Oxidized Phases in Cu under CO Reduction Conditions. *ACS Energy Lett* **2019,** *4* (3), 803-804.
40. Lei, Q.; Zhu, H.; Song, K.; Wei, N.; Liu, L.; Zhang, D.; Yin, J.; Dong, X.; Yao, K.; Wang, N.; Li, X.; Davaasuren, B.; Wang, J.; Han, Y., Investigating the Origin of Enhanced C_{2+} Selectivity in Oxide-

/Hydroxide-Derived Copper Electrodes during CO_2 Electroreduction. *J. Am. Chem. Soc.* **2020**, *142* (9), 4213-4222..
41. Huang, Y.; Chen, Y.; Cheng, T.; Wang, L.-W.; Goddard, W. A., Identification of the Selective Sites for Electrochemical Reduction of CO to C_{2+} Products on Copper Nanoparticles by Combining Reactive Force Fields, Density Functional Theory, and Machine Learning. *ACS Energy Lett* **2018,** *3* (12), 2983-2988.
42. Tang, W.; Peterson, A. A.; Varela, A. S.; Jovanov, Z. P.; Bech, L.; Durand, W. J.; Dahl, S.; Norskov, J. K.; Chorkendorff, I., The importance of surface morphology in controlling the selectivity of polycrystalline copper for CO_2 electroreduction. *Phys. Chem. Chem. Phys.* **2012,** *14* (1), 76-81.
43. Chiang, C.-C.; Chen, M.-C.; Li, L.-J.; Wu, Z.-C.; Jang, S.-M.; Liang, M.-S., Effects of O_2-and N_2-plasma treatments on copper surface. *Japn. J. Appl. Phys.* **2004,** *43* (11R), 7415.
44. Fatyeyeva, K.; Dahi, A.; Chappey, C.; Langevin, D.; Valleton, J.-M.; Poncin-Epaillard, F.; Marais, S., Effect of cold plasma treatment on surface properties and gas permeability of polyimide films. *RSC Adv.* **2014,** *4* (59), 31036-31046.
45. Deng, Y. L.; Handoko, A. D.; Du, Y. H.; Xi, S. B.; Yeo, B. S., In Situ Raman Spectroscopy of Copper and Copper Oxide Surfaces during Electrochemical Oxygen Evolution Reaction: Identification of Cu-III Oxides as Catalytically Active Species. *ACS Catal.* **2016,** *6* (4), 2473-2481.
46. Clark, E. L.; Resasco, J.; Landers, A.; Lin, J.; Chung, L.-T.; Walton, A.; Hahn, C.; Jaramillo, T. F.; Bell, A. T., Standards and Protocols for Data Acquisition and Reporting for Studies of the Electrochemical Reduction of Carbon Dioxide. *ACS Catal.* **2018,** *8* (7), 6560-6570.
47. Ringe, S.; Clark, E. L.; Resasco, J.; Walton, A.; Seger, B.; Bell, A. T.; Chan, K., Understanding cation effects in electrochemical CO2 reduction. *Energy Environ. Sci.* **2019,** *12* (10), 3001-3014.
48. Peterson, A. A.; Abild-Pedersen, F.; Studt, F.; Rossmeisl, J.; Norskov, J. K., How copper catalyzes the electroreduction of carbon dioxide into hydrocarbon fuels. *Energy Environ. Sci.* **2010,** *3* (9), 1311-1315.
49. Garza, A. J.; Bell, A. T.; Head-Gordon, M., Mechanism of CO_2 Reduction at Copper Surfaces: Pathways to C2 Products. *ACS Catal.* **2018,** *8* (2), 1490-1499.
50. Zheng, Y.; Vasileff, A.; Zhou, X.; Jiao, Y.; Jaroniec, M.; Qiao, S. Z., Understanding the Roadmap for Electrochemical Reduction of CO_2 to Multi-Carbon Oxygenates and Hydrocarbons on Copper-Based Catalysts. *J. Am. Chem. Soc.* **2019,** *141* (19), 7646-7659.
51. Malkani, A. S.; Dunwell, M.; Xu, B., Operando Spectroscopic Investigations of Copper and Oxide-Derived Copper Catalysts for Electrochemical CO Reduction. *ACS Catal.* **2019,** *9* (1), 474-478.
52. Cheng, T.; Xiao, H.; Goddard, W. A., Nature of the Active Sites for CO Reduction on Copper Nanoparticles; Suggestions for Optimizing Performance. *J. Am. Chem. Soc.* **2017,** *139* (34), 11642-11645.
53. Zhao, Z. L.; Chen, Z. Z.; Zhang, X.; Lu, G., Generalized Surface Coordination Number as an Activity Descriptor for CO_2 Reduction on Cu Surfaces. *J. Phys. Chem. C* **2016,** *120* (49), 28125-28130.
54. Hori, Y.; Murata, A.; Takahashi, R., Formation of hydrocarbons in the electrochemical reduction of carbon dioxide at a copper electrode in aqueous solution. *J. Chem. Soc., Faraday Trans. 1 F* **1989,** *85* (8), 2309-2326.
55. Weng, L. C.; Bell, A. T.; Weber, A. Z., Towards membrane-electrode assembly systems for CO_2 reduction: a modeling study. *Energy Environ. Sci.* **2019,** *12* (6), 1950-1968.
56. Hori, Y.; Takahashi, R.; Yoshinami, Y.; Murata, A., Electrochemical Reduction of CO at a Copper Electrode. *J. Phys. Chem. B* **1997,** *101* (36), 7075-7081.
57. Resasco, J.; Lum, Y.; Clark, E.; Zeledon, J. Z.; Bell, A. T., Effects of Anion Identity and Concentration on Electrochemical Reduction of CO_2. *ChemElectroChem* **2018,** *5* (7), 1064-1072.
58. Chen, Y.; Huang, Y.; Cheng, T.; Goddard, W. A., Identifying Active Sites for CO_2 Reduction on Dealloyed Gold Surfaces by Combining Machine Learning with Multiscale Simulations. *J. Am. Chem. Soc.* **2019,** *141* (29), 11651-11657.

Table of Contents Graphic